

Nonlinear optics via double dark resonances

S. F. Yelin,¹ V. A. Sautenkov,^{2,3} M. M. Kash,^{4,3} G. R. Welch,³ and M. D. Lukin⁵

¹*Department of Physics, University of Connecticut, Storrs, CT 06269*

²*Lebedev Physics Institute, Moscow, 117924, Russia*

³*Department of Physics, Texas A&M University, College Station, TX 77843*

⁴*Department of Physics, Lake Forest College, Lake Forest, Illinois 60045*

⁵*Department of Physics, Harvard University, Cambridge, MA 02138*

(Dated: November 3, 2018)

Double dark resonances originate from a coherent perturbation of a system displaying electromagnetically induced transparency. We experimentally show and theoretically confirm that this leads to the possibility of extremely sharp resonances prevailing even in the presence of considerable Doppler broadening. A gas of ⁸⁷Rb atoms is subjected to a strong drive laser and a weak probe laser and a radio frequency field, where the magnetic coupling between the Zeeman levels leads to nonlinear generation of a comb of sidebands.

I. INTRODUCTION

Dark resonances arise from the quantum superposition states that are decoupled from coherent and dissipative interactions. They are now a well-known concept in quantum optics and laser spectroscopy, leading to concepts such as electromagnetically induced transparency (EIT) [1], lasing without inversion and increased resonant index of refraction [2], highly efficient resonant nonlinear optics [3, 4, 5], “slow” light [6, 7, 8, 9], coherent storage of photon states [10, 11, 12], and femto-second generation [13, 14].

As a rule, any perturbation of the dark state leads to undesirable decoherence. However, it was shown theoretically that “perturbing” the dark state coherently leads to multiple quantum superposition states that interact coherently. These so-called “double-dark” states [15, 16] can be used to mitigate decoherence effects and thus enlarge the domain of dark state physics. The perturbation can come from different sources: microwave or optical coherent fields, DC-fields, non-adiabatic optical coupling (i.e. effective fields). In this paper we discuss theoretically and experimentally the use of the magnetic component of a radio frequency (RF) field. We observe two sharp resonances at shifted frequencies. We also demonstrate that the double dark resonances allow to enhance the nonlinear optical process. In particular, we demonstrate the efficient generation of a comb of multiple frequency components associated with double dark resonances.

II. THEORY

A. Dark resonances and electromagnetically induced transparency

The principle of electromagnetically induced transparency (EIT) is the destructive interference of two absorption channels, which originate from a Stark split resonance. It is based on a so-called *dark resonance*: For

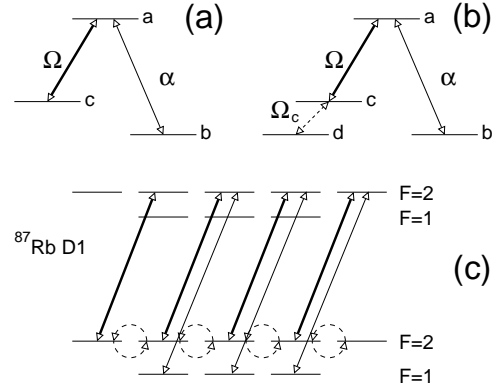


FIG. 1: (a) Energy level scheme of a Λ -system. (b) Extension of (a) by an additional weak coherent field Ω_c to a four-level system. (c) “Four level” system in ⁸⁷Rb as used in the experiment.

example, in a Λ -system like the one in Fig. 1a with the excited state $|a\rangle$ coupled to the metastable states $|b\rangle$ and $|c\rangle$ via strong driving and weak probe fields with Rabi frequencies Ω and α , respectively, the resonant interaction Hamiltonian is $H = \hbar\Omega|c\rangle\langle a| + \hbar\alpha|b\rangle\langle a| + \text{H.c.}$. The superposition state $|+\rangle \propto \Omega|c\rangle + \alpha|b\rangle$ is coupled by both fields, $H = \hbar\Omega_+|+\rangle\langle a| + \text{H.c.}$, with $\Omega_+^2 = \Omega^2 + \alpha^2$, whereas the orthogonal state $|-\rangle \propto \Omega|b\rangle - \alpha|c\rangle$ is *dark*, and $H|-\rangle = 0$. This is true as long as the probe and driving fields are in two-photon resonance with the transition $|b\rangle \leftrightarrow |c\rangle$. If all the atoms in the medium are in the dark state the medium is transparent to both fields (see probe spectrum in Fig. 2 (broken line)).

B. Double-dark resonances

The usual mechanism by which perturbing the dark state destroys the transparency has been reviewed recently [15]: Here we show that a coherent perturbation, e.g., a weak monochromatic electromagnetic field with Rabi frequency Ω_c coupling an additional state (see

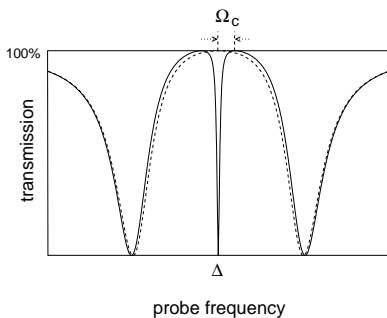


FIG. 2: Transmission spectrum (dashed line) of probe field \mathcal{E} of Fig. 1a if the drive field Ω is on resonance. The probe field is resonant at the center of the figure. The solid line depicts the same transmission spectrum in the presence of an additional weak coherent perturbation (cf. Fig. 1b). The transparency is split by $2\Omega_c$.

Fig.1b), can display interesting and highly coherent features. This case is depicted in Fig. 2 (solid line), where a sharp absorption line appears on resonance, that splits the point of transparency in two. The two transmission maxima are now detuned by $\pm\Omega_c$. This absorption line can be very narrow, as its width scales with the ratio of the intensities Ω_c^2/Ω^2 . Nevertheless, its depth shows that the resonant absorption is as strong as that of the original Stark-split levels. For a simplified explanation of this phenomenon, the dressed-state picture is very useful, where the Hamiltonian is diagonalized with respect to driving and perturbing fields. The resulting resonant state, $|0\rangle \approx |d\rangle + \Omega_c/\Omega |a\rangle$, has a small admixture of the excited state, and thus it decays very slowly, which results in a very narrow resonance. In this picture, it is easy to prove that in the all-resonant case, detuning the field Ω_c by Δ_{RF} implies a frequency shift of the novel resonance line by Δ_{RF} .

C. Model

The experiment described in this article follows a slightly different setup: The states $|c\rangle$ and $|d\rangle$ are degenerate (i.e., Zeeman sublevels), whereas the new field, a radio frequency (RF) field, has the fixed frequency ν_{RF} . This situation is the same as if there were two novel fields that are blue and red detuned by $\pm\Delta_{\text{RF}} = \nu_{\text{RF}}$. One can thus expect two novel lines with half the absorption depth, shifted by $\pm\nu_{\text{RF}}$ compared to the center, as in Fig. 3a (inset).

In order to understand this behavior, we investigate briefly the dressed state system (i.e., the eigenvalues/eigenstates of the atom + drive + RF - system)(cf. Fig. 4): The Hamiltonian of this setup (in the interaction picture without the probe field) is

$$H = \hbar\Omega |a\rangle \langle c| + \frac{\hbar}{2}\Omega_c (|d_1\rangle \langle c| + |d_2\rangle \langle c|) + H.c. + \hbar\Delta_{\text{RF}} (|d_1\rangle \langle d_1| - |d_2\rangle \langle d_2|). \quad (1)$$

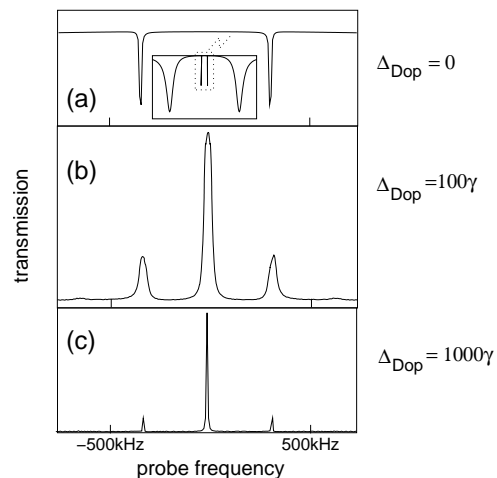


FIG. 3: (a) Transmission spectrum as in Fig. 1b, but for a situation in which $|c\rangle$ and $|d\rangle$ have the same energy, and the additional field is a fixed-frequency RF field. The main figure is a blowup of the inset. (b) Same as (a), but with a (realistic) Doppler broadening of $\Delta_{\text{Dop}} \sim 500$ MHz, which is approximately 100 natural linewidths of the probe transition. (c) Same as in (b), but with ten times higher Doppler broadening, in order to demonstrate the Doppler narrowing effect.

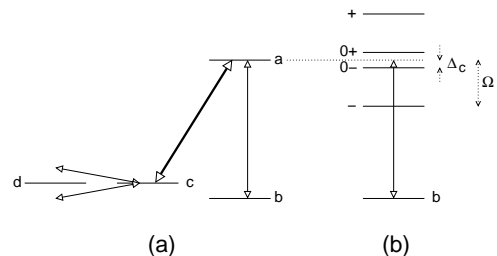


FIG. 4: (a) Simple level system of the double dark setup as used in our experiment, where the RF field can be seen as red and blue detuned. (b) Same system, but in a dressed state picture. The level $|d\rangle$ is split into two by the red and blue detuned RF components, whereas the dressed states $|+\rangle$ and $|-\rangle$ are nearly the same as in a simple Λ -system.

Here, $|d\rangle$ is split into $|d_1\rangle$ and $|d_2\rangle$ to include the fact that the RF field is red and blue detuned at the same time. From this Hamiltonian we find the dressed state system

$$|\pm\rangle \approx \frac{1}{\sqrt{2}} (|a\rangle \pm |c\rangle) \quad (2)$$

with

$$\lambda_{\pm} \approx \pm\Omega$$

and

$$|0_{\pm}\rangle \approx |d_{1/2}\rangle + \frac{\Omega_c}{2\Omega} f(\Omega, \Delta_{\text{RF}}) \left(\pm |a\rangle + \frac{\Delta_{\text{RF}}}{\Omega} |c\rangle \right) \quad (3)$$

with

$$\lambda_{0\pm} \approx \pm\Delta_{\text{RF}}$$

Here we use $f(\Omega, \Delta_{\text{RF}}) = \Omega^2/(\Omega^2 - \Delta_{\text{RF}}^2)$ and assume $\Omega \neq \Delta_{\text{RF}}$. The small admixture of the excited state

makes sure that the dressed states $|0\pm\rangle$, replacing $|d\rangle$, decay with a very narrow linewidth, and the eigenenergies coincide directly with the frequencies of the absorption lines.

D. Nonlinear sideband generation

This arrangement also produces efficient nonlinear modulation: sidebands appear in even multiples of the RF frequency ν_{RF} . This can be explained the following way: Two RF photons couple (via state $|d\rangle$) to virtual states $|c_{2\pm}\rangle$, that are lying exactly $2\nu_{RF}$ above and below the level of $|c\rangle$ (see Fig. 5). The driving field parametrically creates a transparency for the probe field at $2\nu_{RF}$ above and below its original frequency. Higher order nonlinearities then can be seen for fourth, sixth, etc., order virtual levels $|c_{4\pm}\rangle$, $|c_{6\pm}\rangle$, etc., with decreasing intensities (see section III C).

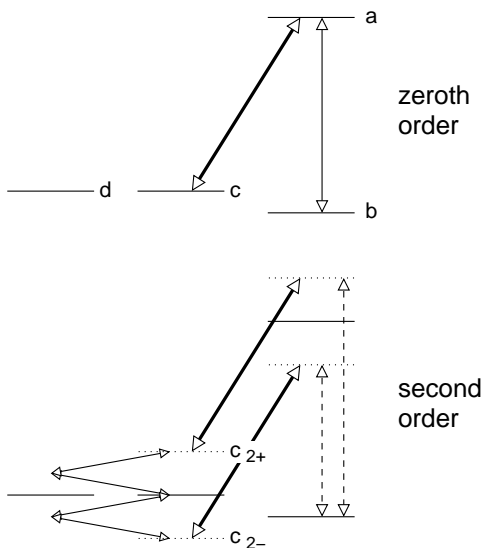


FIG. 5: Level structure illustrating how a non-resonant (i.e., finite-frequency) RF field can generate second order frequencies. The solid levels are pure atomic states, the dashed ones are virtual states created by the fields. The solid field arrows designate in- and outgoing fields, whereupon the dashed arrows signify fields that are created parametrically, and thus only outgoing.

E. Doppler narrowing

The experiment is performed in a hot gas and therefore Doppler broadening is an important consideration. We will give here a brief explanation of the impact of Doppler shifts, as they pose an interesting puzzle. For each velocity component of the atomic gas, the probe and drive transitions are affected by Doppler shifts equally, since these shifts depend linearly on the frequency and probe and drive fields copropagate. The RF transition,

however, is essentially unaffected because of its very low frequency. It can be expected that the transparency on resonance in the Doppler-broadened case gives rise to a transparency whose width decreases for increasing Doppler broadening. Surprisingly, there are Doppler narrowed *transmission* lines replacing the absorption lines of the Doppler free case. This ‘‘Doppler narrowing’’ can be explained using Fig. 6.

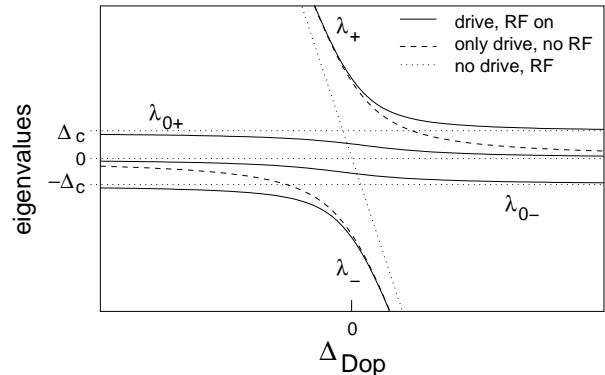


FIG. 6: Eigenvalues of the system as a function of the Doppler shift Δ_{Dop} , i.e., for all different velocity groups. The eigenvalues in this figure depict the true energy level of the atomic states, and therefore would be at the center of any absorption line, whereas transmission would be visible somewhere between the eigenvalues. Dotted lines depict the energy levels of the atomic states when neither the drive (Ω) nor the RF field (Ω_c) is present. The broken lines are for $\Omega_c = 0$, but $\Omega \neq 0$. The solid lines give the solution for all three fields, RF, drive and probe, present.

For each velocity group there are 4 eigenvalues in the system. Each eigenvalue is responsible for an absorption line. In the limit of vanishing RF field, and with the probe and drive fields on resonance for the zero velocity group $\Delta_{Dop} = 0$, they are

$$\lambda_{0\pm}^{Dop} = \pm\Delta_{RF},$$

$$\lambda_{\pm}^{Dop} = \frac{\Delta_{Dop}}{2} \pm \sqrt{\frac{\Delta_{Dop}^2}{4} + \Omega^2},$$

where Δ_{Dop} is the Doppler frequency shift. Shown in Fig. 6 are the energy eigenvalues λ_{\pm}^{Dop} and $\lambda_{0\pm}^{Dop}$ of the atomic dressed states as functions of the Doppler shift Δ_{Dop} . Eigenvalues λ_{\pm}^{Dop} (shown in the figure as broken lines) are responsible for the Stark split absorption lines in usual EIT. The dotted lines show all eigenvalues without both, driving and RF fields ($\Omega = \Omega_c = 0$. Note that in this case there are no avoided crossings.) With both fields present all anticrossings appear in Fig. 6 (solid lines). Performing the Doppler average over all components (which in mathematical terms means a Gaussian average over all Δ_{Dop}) leads to an absorption profile where narrow transparency lines can be seen very close to the $\pm\Delta_{RF}$ eigenvalues. The reason is obvious from Fig. 6, where the regions very close to $\pm\Delta_{RF}$ and to 0 are the

only ones that are not crossed by any of the eigenvalues over the width of all Δ_{Dop} . Thus these lines are nearly at the frequency where there is maximum absorption in the Doppler free case, and become narrower the broader the Doppler shift is spread.

The resulting transmission curve can be seen in the simulation of Fig. 3, where the three lines, (one EIT and two double dark lines) are clearly visible. The parameters in (b) are chosen to coincide with the experimental reality: The Doppler broadening in our experiment is 530 MHz.

The sideband generation is much more pronounced in the Doppler broadened medium than in the non-broadened one, which seems surprising at first. It helps to remember that the RF novel lines are absorption resonances in the non-broadened case, whereas they are transmission resonances in the Doppler broadened case. These transmission lines coincide with the zero-order dark resonance lines of the sideband spectra (see, e.g., Fig. 9). The consequence is that the ratio of neighboring sideband intensities $I_{4\Delta_{\text{RF}}}/I_{2\Delta_{\text{RF}}} \approx I_{2\Delta_{\text{RF}}}/I_0$ is roughly two orders of magnitude higher for Doppler broadened media, such that the three-peak structure of the fundamental mode can also be seen in the second order sidebands (Fig. 9(a,b)).

III. EXPERIMENT

A. Setup

The experiment was performed on the D_1 resonance line of ^{87}Rb (nuclear spin $I=3/2$, wavelength 795nm). The experimental setup is shown in Fig. 7. In our experiment, external cavity diode lasers (ECDL) were used for

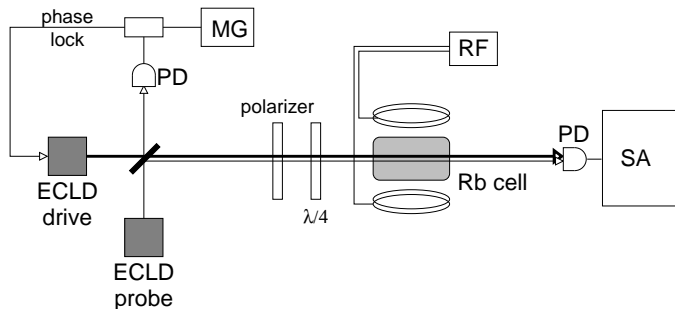


FIG. 7: Experimental setup. The drive and probe fields are produced by phase-locked extended cavity laser diodes (ECLD) and σ_+ -polarized by a polarizer and $\lambda/4$ -wave plate. A spectrum analyzer (SA) examines the probe-drive beat note. The weak coupling field is produced by a radio frequency (RF) coil.

both the drive and the probe fields. The two collinear beams, both of which are circularly polarized and which have the same diameter of 0.1 cm are overlapped and directed into a glass cell of length $l = 4$ cm, filled with

rubidium vapor. The vapor consisted of $4 \times 10^{11}\text{cm}^{-3}$ ($T = 65^\circ\text{C}$) of the natural abundance of ^{85}Rb and ^{87}Rb , plus 3 Torr of Ne buffer gas. The buffer gas is needed in order to reduce the relaxation rate of the ground state coherence, which for vapor densities of this order stems mostly from the Rb atoms entering into and leaving the interaction region with the laser beams. Thus the ground state decoherence rate depends on the diameter of the laser beams and in our case can be estimated to be of the order of 5 kHz. The cell was mounted inside a three-layered magnetic shield. Perpendicular to the laser beams the RF field could be applied, using transverse coils. The amplitude of the magnetic component of the RF field is chosen such that it is of the order 0.1 G. The cell was heated using DC current in a high-resistance wire wound on the outside of the middle shield. The atomic density can then be estimated from the temperature in the cell using well-known vapor-pressure curves, e.g. from [17]. The drive laser was tuned to the $5S_{1/2}(F=2) \leftrightarrow 5P_{1/2}(F=2)$ transition; the probe laser was tuned to the $5S_{1/2}(F=1) \leftrightarrow 5P_{1/2}(F=2)$ transition. This configuration of drive and probe fields creates an appropriate Λ -system within the ^{87}Rb D1 manifold (see Fig. 1c).

There must be minimal relative laser jitter between probe and drive fields, so the probe laser was phase-locked to the driving field frequency with an offset frequency of 6.8 GHz, which is equal to the hyperfine ground state splitting between the $5S_{1/2}(F=1)$ and $5S_{1/2}(F=2)$ states. This offset is fixed by a tunable microwave frequency synthesizer. After passing through the cell the laser beams hit a fast photodiode. The beat signal from this photodiode is monitored by a microwave spectrum analyzer, which is used as a broadband filter-amplifier with a bandwidth of 3 MHz, centered at the hyperfine splitting frequency.

B. Spectrum

The lineshape of the dark resonances are then determined by scanning the probe laser frequency, which was accomplished by tuning the frequency of the synthesizer. While the laser power of the driving field can be changed from 0 to 6 mW, the probe laser was held at 1% of the drive power. With these parameters a broadening of the dark resonances could be observed with a slope of 30 kHz/mW. Field broadening and density narrowing of the dark resonance were investigated in Ref. [18]. In order to observe EIT resonance and pronounced double dark structure, the driving field had to be strong enough to make the the additional double dark structures lie well within the EIT resonance. (As was tested experimentally in this scope, the novel features are not visible otherwise.) The optimal working point thus was determined to be 2.2 mW for the drive laser.

The double dark resonance structures can be seen in Fig. 8a. These additional resonances are induced by the

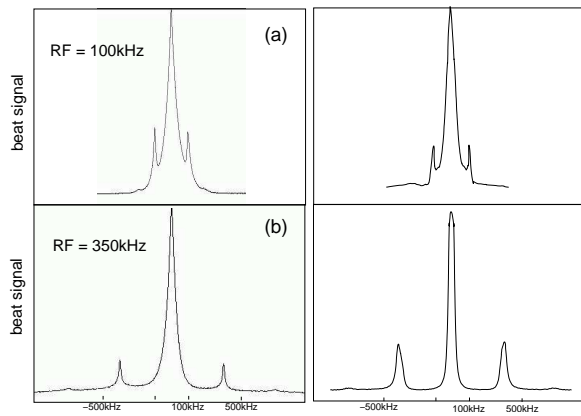


FIG. 8: Transmission curves for two different RF frequencies, experiment (right) and theory (left). In (a) the RF is 100 kHz, where the new resonances still overlap with the dark resonance peak, whereas in (b), with a RF of 350 kHz, these lines are well resolved. The RF magnetic field component in these curves was 20 mG in (a) and 80 mG in (b).

alternating magnetic field with a frequency of 100 kHz. An RF field with a frequency of 350 kHz is shown in Fig. 8b. The new transparency lines are well outside the EIT peak. As can be seen in the figures, the frequency interval between the dark resonance and the new resonances indeed equals the RF frequency. The width of the novel resonances is 20 kHz, which suggests a total decoherence rate between the three ground states $|b\rangle$, $|c\rangle$, and $|d\rangle$ of 20 kHz.

C. Sideband generation

The spectral distribution of the transmitted laser light was also studied. For this purpose the spectrum analyzer was switched to a narrow band regime (bandwidth 30 kHz) and the central frequency of the bandwidth was scanned. The laser frequency during the spectrum analyzer scan was fixed. In this procedure several new optical components (sidebands) can be observed, which are separated by frequency intervals equal to harmonics of the applied magnetic field frequency. Obviously these optical components are generated during the propagation of laser light through the coherently prepared Rb vapor. In order to record their dependence on the laser frequency, we present snapshots where frequency steps of 20 kHz are taken, see Fig. 9.

The fundamental frequency here is the frequency of the beat-note of the drive- and probe- laser beams without the cell. The signal at the fundamental frequency is similar to the broadband detected signal in Fig. 8b, as could be expected. One can see the different behavior of the odd and even harmonics (sidebands). The amplitude of the second order sidebands that are observed at ± 700 kHz is higher than the the amplitude of the first order sidebands that are observed at ± 350 kHz. The

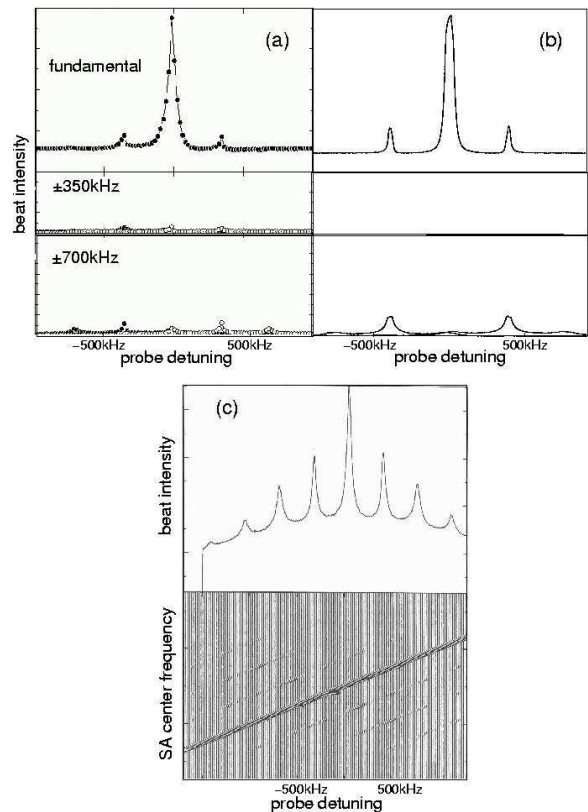


FIG. 9: (a) Spectrum of the drive-probe beat note transmission. In the upper picture, the spectrum analyzer (SA) is centered around the fundamental, i.e., resonance frequency. In the two lower graphs, the SA is tuned to the first and second order sidebands, respectively. It is clear from these curves that only even order sidebands are supported. (b) Simulations of curves in (a). Note that while in theory there are no first order sidebands, there are small ones in the experimental data. (The reason for that is a broad fundamental mode.) (c) The upper curve is similar to the one in (a), but with much stronger RF fields (160 mG) such that multiple sidebands are visible. This spectrum is an integration over all SA frequencies. The resolution by SA frequencies is given in the lower picture.

reason that they are seen at all stems from the fact that the fundamental mode is broad enough to seep into the first order sidebands. In this case, the virtual states $|d_{\pm}\rangle$, detuned by $\pm\Delta_{\text{RF}}$ from state $|d\rangle$, are directly coupled to $|a\rangle$, which leads to first order sidebands. Note that in the simulations (Fig. 3) no first order sidebands are present.

The three-peak structure in the main diagonal of the lower curves of Fig. 9(c) is the main contribution to the integrated spectrum (upper curve), and for low RF intensities is all that is seen (e.g., in (a,b)). In reality, however, this contribution makes up only the fundamental mode. Sidebands originate in the resonances with $|c_{2\pm}\rangle$, $|c_{4\pm}\rangle$, etc., and can be seen for stronger RF intensity, such as in Fig. 9(c). There, each of the diagonals, which are offset from their neighbors by $\pm 2\nu_{\text{RF}}$, consists of the fundamental three-peak structure. Finally, in the integrated

picture they add up to the multi-peak spectrum in the upper curve.

IV. CONCLUSION

In conclusion, we have experimentally demonstrated novel coherent resonances as predicted in Ref. [15]. These novel resonances are very sharp and highly sensitive to frequency and intensity of a RF field, which perturb the dark resonance. In addition, because of higher-order

coupling, efficient non-linear sideband generation was demonstrated. This scheme can be used in applications like sensitive nonlinear measurements such as Ref. [19] and UV laser generation [20].

We want to thank M. O. Scully for his interest in this project and discussions leading to it, and we want to thank the Office of Naval Research and the National Science Foundation for support. SFY also acknowledges a Feodor-Lynen Fellowship from the Humboldt Foundation.

-
- [1] S. Harris, *Physics Today* **50**, 36 (1997), for review.
 - [2] M. O. Scully and M. S. Zubairy, *Quantum optics* (Cambridge, University Press, Cambridge, 1997), for references.
 - [3] A. J. Merriam, S. J. Sharpe, M. Shverdin, D. Manuszak, G. Y. Yin, and S. E. Harris, *Phys. Rev. Lett.* **84**, 5308 (2000).
 - [4] M. D. Lukin and A. Imamoglu, *Phys. Rev. Lett.* **84**, 1419 (2000).
 - [5] P. R. Hemmer, D. P. Katz, J. Donoghue, M. Cronin-Golomb, M. S. Shahriar, and P. Kumar, *Opt. Lett.* **20**, 982 (1995).
 - [6] L. V. Hau, S. E. Harris, Z. Dutton, and C. H. Behroozi, *Nature* **397**, 594 (1999).
 - [7] M. M. Kash, V. A. Sautenkov, A. S. Zibrov, L. Hollberg, G. R. Welch, M. D. Lukin, Y. Rostovtsev, E. S. Fry, and M. O. Scully, *Phys. Rev. Lett.* **82**, 5229 (1999).
 - [8] D. Budker, D. F. Kimball, S. M. Rochester, and V. V. Yashchuk, *Phys. Rev. Lett.* **83**, 1767 (1999).
 - [9] O. Kocharovskaya, Y. Rostovtsev, and M. O. Scully, *Phys. Rev. Lett.* **86**, 628 (2001).
 - [10] C. Liu, Z. Dutton, C. H. Behroozi, and L. V. Hau, *Nature* **409**, 490 (2001).
 - [11] D. Phillips, A. Fleischhauer, A. Mair, R. Walsworth, and M. D. Lukin, *Phys. Rev. Lett.* **86**, 783 (2001).
 - [12] R. L. Walsworth, S. F. Yelin, and M. D. Lukin, *Opt. Phot. News. May Issue*, 50 (2002), and refs therein.
 - [13] S. E. Harris and A. V. Sokolov, *Phys. Rev. Lett.* **81**, 2894 (1998).
 - [14] K. Hakuta, L. Marmet, and B. P. Stoicheff, *Phys. Rev. A* **45**, 5152 (1992).
 - [15] M. D. Lukin, S. F. Yelin, M. Fleischhauer, and M. O. Scully, *Phys. Rev. A* **60**, 3225 (1999).
 - [16] C. Y. Ye, A. S. Zibrov, Y. V. Rostovtsev, and M. O. Scully, *Phys. Rev. A* **65**, 043805 (2002).
 - [17] A. N. Nemeyanov, *Vapor pressure of chemical elements* (Elsevier, Amsterdam, 1963).
 - [18] V. A. Sautenkov, M. M. Kash, V. L. Velichansky, and G. R. Welch, *Laser Physics* **9**, 889 (1999).
 - [19] S. F. Yelin and P. R. Hemmer, *Phys. Rev. A* **66**, 013803 (2002).
 - [20] E. S. Fry, M. D. Lukin, T. Walther, and G. R. Welch, *Opt. Comm.* **179**, 499 (2000).